Nanoscale

Accepted Manuscript

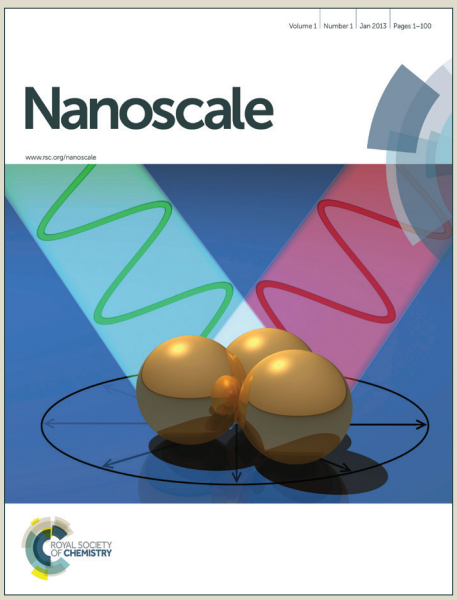

ROYAL SOCIETY OF CHEMISTRY

www.rsc.org/nanoscale

Nanoscale

RSCPublishing

ARTICLE

Bias-free, Solar-charged Electric Double-Layer Capacitors

Cite this: DOI: 10.1039/x0xx00000x

Hao Wu,† Jing Geng,† Yuhang Wang, Yanli Wang, Zheng Peng, and Gengfeng Zheng*

Received 00th January 2012,
Accepted 00th January 2012

DOI: 10.1039/x0xx00000x

www.rsc.org/

The conversion of solar energy with simultaneous electric energy storage provides a promising means for optimizing energy utilization efficiency and reducing device volume. In this paper, a 3-dimensional mesoporous carbon coated branched TiO_2 nanowire composite is rationally designed for direct conversion and storage of solar energy as electric double-layer capacitive energy. The 1-dimensional, crystalline TiO_2 trunks serve as long light absorption and continuous charge transport pathways, and the high-density TiO_2 branches can efficiently increase the contact area with the surface coated mesoporous carbon layers. In addition, the ordered and uniformed mesopores provide large pore sizes for electrolyte penetration, and high surface area for charge absorption and storage. Under a 1-sun illumination and no external electric bias, this branched TiO_2/mesoporous carbon composite exhibits specific capacitances of over 30 and 23.4 F/g, at current densities of 0.1 and 0.5 A/g, respectively. An excellent stability of > 50 photocharging-electrical discharging cycles has also been demonstrated, suggesting the potential of further developing this hybrid material structure for simultaneous solar conversion and electric energy storage.

Introduction

Electric double-layer capacitors (EDLCs) are important device structures for efficient energy storage,[1-10] for which carbon nanostructures, such as carbon nanoparticles,[1] nanotubes,[2,3] and graphene,[4,5] are among the most promising candidates capable of offering high power density and capacitances. Mesoporous carbon materials, synthesized by surfactant-directed organic-organic self-assembly, have also attracted substantial research interest for developing EDLCs recently,[6-10] due to their remarkable properties including high specific surface area, tunable pore size, ordered mesostructure, high conductivity and chemical stability.[6-11] Nonetheless, all the EDLCs reported so far are charged by external electrical power sources, which limit their potential utilization in portable devices.

On the other hand, solar energy represents as a clean, unlimited, and widely available energy source, and has been substantially investigating for developing alternative energy supply, such as solar cells,[12-16] photoelectrochemical (PEC) cells and photocatalysis.[17-30] Nonetheless, almost all the previous solar energy-based reports are aimed for developing electric cells that provide optimal output voltage and current, while the storage of the electric energy is carried out in a separate cell, resulting in increase of design complexity, device size as well as loss of electric energy over the external circuit.[17-27] Xia *et al*. reported an integrated PEC-pseudocapacitor device design by depositing a layer of metal hydroxides/oxides on TiO_2 surface,[31] while an external electric field is still needed to drive the photogenerated electrons from the TiO_2 conduction band for water reduction. Recently, our group demonstrated a fully solar energy-powered PEC conversion for simultaneous solar energy conversion and electric energy storage,[32] using Pt nanoparticle-decorated Si nanowires (NWs) as photocathode and $Ni(OH)_2$ nanoparticle-coated TiO_2 NWs as photoanode. A discharging capacitance of ~ 455 F/g is obtained for the first discharging cycle, which gradually decreases at subsequent cycles due to the dissolution of $Ni(OH)_2$ over the charging/discharging process. In spite of these research progresses, an integrated photoelectric conversion/EDLC energy storage device, with fully solar energy driven capability and excellent cycling stability, has yet to be realized.

Herein, we developed a hybrid, 3-dimensional (3D) composite of branched TiO_2 NWs coated with mesoporous carbon layers (branched-TiO_2/meso-C), for unassisted solar-based PEC conversion and electric capacitive energy storage. As schematically shown in Fig. 1a, the 3D branched TiO_2 NW cores not only possess 1D conducting channels for rapid electron-hole separation and charge transport, but also provide long optical paths for efficient light absorption and high surface areas for fast charge transfer rate and electrochemical reactions

at interfaces, thus serving as an excellent candidate for photoanode.[23-26] In addition, a mesoporous carbon layer coated over the branched TiO_2 NW arrays offers high surface area (608 m^2/g) for charge absorption, tunable pore size (~ 15 nm) for effective electrolyte transport, and excellent chemical inertness for long cycling life.[6-10] Thus, the photogenerated electron-hole pairs are separated on the surface of branched-TiO_2 nanowires, where electrons flow to the Pt counter electrode and generate hydrogen, and holes diffuse onto the coated meso-C surface, and the hydroxyl ions in the solution serve as the counter ions (Fig. 1b).[33, 34] As a proof-of-concept, under a simulated sunlight of 100 mW/cm^2 without any additional applied potential, this branched-TiO_2/meso-C hybrid structure exhibits an output voltage of 0.125 V, and stable specific capacitances of 30 and 23.4 F/g at discharge current densities of 0.2 and 0.5 A/g, respectively, which is 3 times higher than that of a similar material design while the mesoporous carbon layer is replaced by non-porous carbon. Furthermore, the 3D branched-TiO_2/meso-C hybrid structure shows a stable cycling performance in solar charging/electrical discharging process, thus suggesting a promising bias-free, solar-charged EDLC structure for simultaneous, direct energy conversion and storage.

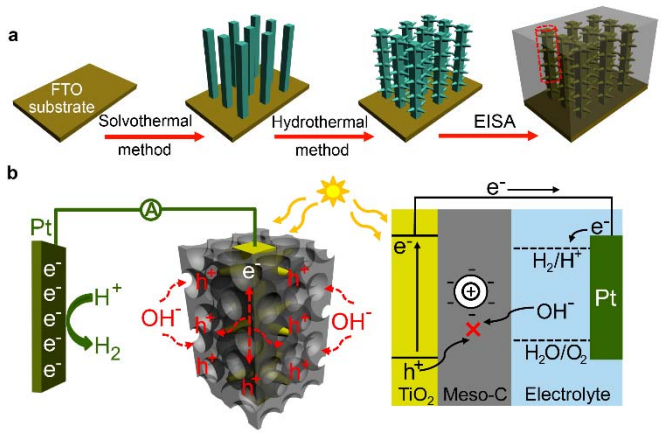

Fig. 1 (a) Schematic of synthesis of the 3D branched-TiO_2/meso-C hybrid structure (See details in Experimental Section). (b) Working principle of direct solar energy conversion and storage, and the energy band diagrams of the system.

Experimental

Synthesis of branched-TiO_2 nanowires

A two-step synthesis was used for the branched-TiO_2 NW growth. In the first step, a modified solvothermal method was used for fabricating one-dimensional (1D) TiO_2 nanowire arrays.[13] In brief, TiO_2 seed was coated on a fluorine-doped tin oxide (FTO) glass substrate by a dip-coating method using 0.3 M tetrabutyl titanate in ethanol as precursor, and followed by annealing at 500 °C in air for 30 min. The substrate was then placed in a 50 mL Teflon-lined stainless steel autoclave containing 10 mL of n-butanone, 10 mL of 37% hydrochloric acid, and 1 mL of tetrabutyl titanate, and was kept at 200 °C for 1 h. Then the sample was washed with ethanol, dipped in a mixture of H_2O_2 (30 wt%) and $NH_3 \cdot H_2O$ (25 wt%) (v/v = 10/1) for 10 min, rinsed with deionized (DI) water and heated at 400 °C in air for 1 h, successively. For the branch growth, the as-obtained NW arrays were placed in a sealed Teflon-lined stainless steel autoclave filled with 20 mL of DI water, 0.5 mL of 37% hydrochloric acid and 0.3 mL of $TiCl_4$ solution, and kept at 80 °C for 1 h. Then the sample was washed with DI water and annealed at 400 °C in air for 1 h.

Synthesis of branched-TiO_2/mesoporous carbon hybrids

A modified evaporation induced self-assembly (EISA) process was used to grow mesoporous carbon layer on branched-TiO_2 NWs.[35] In a typical synthesis, 0.3 g of Pluronic F127 (poly(ethylene oxide)-b-poly(propylene oxide)-b-poly(ethylene oxide), EO_{106}-PO_{70}-EO_{106}, M_w = 12,600, Sigma-Aldrich Co. LLC.) was dissolved in 2.16 g of ethanol, and mixed with 3 g of phenolic resol (20 % in ethanol, Sigma Aldrich Co. LLC.) by stirring over 30 min to form a homogeneous solution. The mixed solution was spin-coated onto the branched-TiO2 nanowire sample, followed by drying at 40 °C for 24 h and then 100 °C for 24 h, respectively. The final hybrid structure was obtained by pyrolyzing to 600 °C a heating rate of 1 °C/min and kept for 3 h at 600 °C in N_2 atmosphere, with a flow rate of 50 cm^3/min. The branched-TiO_2/carbon sample was obtained in an otherwise similar approach, without adding F127 in the precursors.

Photoelectrochemical measurement

All electro-chemical measurements were performed under three-electrode configuration in 1 M KOH electrolyte with Ag/AgCl as the reference electrode and Pt foil as the counter electrode in a Metrohm Autolab electrochemical workstation. The charging process was performed under 1-sun (100 mW/cm^2) illumination irradiating from the back side (without active materials), without external electric bias. The discharging process was carried out under galvanostatic mode without illumination. The specific capacitance was calculated according to the equation: $C = I \Delta t / (M \Delta V)$, where C (F/g), I (A), Δt (s), M (g), and ΔV (V) represented the discharge current, the discharging time, the mass of active materials (carbon or mesoporous carbon), and the potential difference during discharging, respectively.[32]

Results and discussion

The synthesis of the 3D branched-TiO_2/meso-C hybrid structure is synthesized by a two-step solvothermal-hydrothermal method,[13,25] followed by an evaporation induced self-assembly approach (Experimental section). After the first solvothermal step, the growth substrate is covered with a layer of need-like NW arrays, with average diameter and length of 80

nm and 4.5 μm, respectively (Fig. S1a, b). After the second hydrothermal step, small branches with an average length of 80 nm and diameters of 10-50 nm are observed to grow on the primary NW trunks (Fig. 2a, b). This highly orientated 3D branched-TiO_2 nanowire structure is beneficial in charge transportation and suppressing electron-hole combination.[23-26] After coating of mesoporous carbon layer on the branched TiO_2 NW arrays by the EISA approach,[35] a mesoporous structure is clearly recognized (Fig 2c, d), which is permeated downward about 3 μm from the top end of the 3D branched-TiO_2 (Fig. S1c, d). Transmission electron microscopy (TEM) images of the branched-TiO_2/meso-C hybrid structure clearly exhibit that the branched TiO_2 nanowires are tightly embedded in an ordered mesoporous carbon framework (Fig. 2e). The mesopore size is measured to be ~ 10–20 nm. High-resolution TEM (HRTEM) images reveal well-resolved lattice fringes of both NW trucks and branches (Fig. 2f), with a lattice constant of 0.249 nm matched with the (101) lattice plane of rutile TiO_2, indicating excellent crystallinity and the epitaxial growth of the TiO_2 branches.

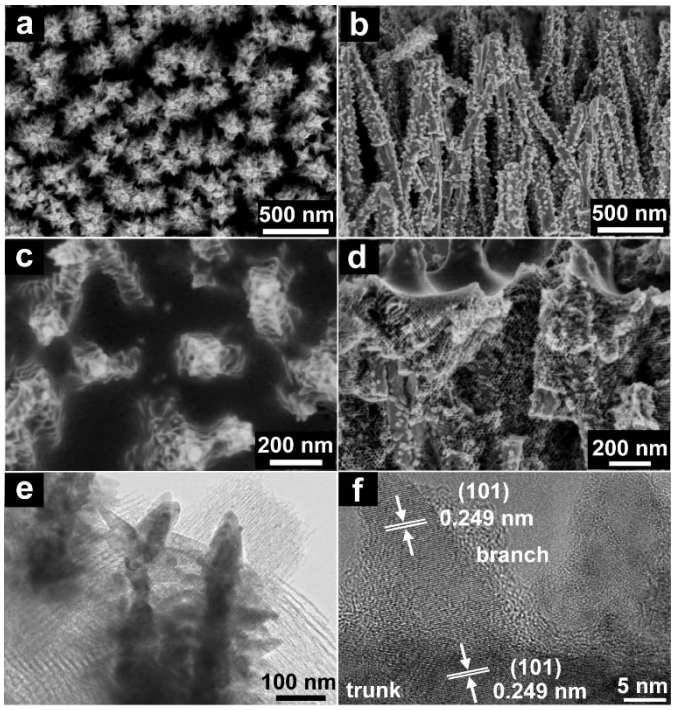

Fig. 2 (a) Top-view and (b) side-view SEM images of 3D branched-TiO_2 nanowire arrays. (c) Top-view, (d) side-view SEM images, (e) TEM and (f) HRTEM images of the branched-TiO_2/meso-C hybrid structure.

X-ray diffraction (XRD) spectroscopy further confirms that the 3D branched-TiO_2 NWs (as well as the 1D TiO_2 NWs without branches) have a tetragonal rutile phase crystal structure (JCPDS No. 73-1232), Fig. S2. Compared to the 1D TiO_2 NWs, a much increase of peak intensity of the (101) crystal facet is observed for 3D branched-TiO_2 NW, due to the increase of branches with exposing (101) crystal facet.[13] N_2 sorption isotherm curves show that the branched-TiO_2/meso-C hybrid structure has a surface area of 35.8 m^2/g (Fig. S3a), which corresponds to a surface area of 608 m^2/g when only the carbon mass is considered, due to the negligible contribution of surface area from the non-porous branched-TiO_2 component. The pore size distribution is calculated to be centered at ~ 15 nm, respectively (Fig. S3b), in good accord with the mesopore size obtained from the TEM results.

To investigate the solar energy-powered electric storage performance of the branched-TiO_2/meso-C hybrid structure, a three-electrode configuration is adopted (Experimental section). Both the branched TiO_2 NWs without carbon coating (designated as branched-TiO_2) and with non-porous carbon coating (designated as branched-TiO_2/C) are also measured under same conditions for comparison. The output potential of the bare branched-TiO_2 NWs increases sharply by 0.39 V under illumination (Fig. 3a), while it increases relatively slowly 0.125 V for the branched-TiO_2/meso-C hybrid structure. The decreases of the output voltage can be attributed to the transfer of photogenerated holes from TiO_2 surface to carbon surface. An even smaller output voltage (~ 0.046 V) is observed for the branched-TiO_2/C composite, which may be ascribed to the further reduction of absorption in the UV region due to the increase of carbon layer density around the branched-TiO_2 NWs (Fig. S4). In addition, the output voltages of both the branched-TiO_2/C (Fig. 3b) and the branched-TiO_2/meso-C structures (Fig. 3c) show an increasing trend with the solar light illumination time, confirming the gradual charge process of the carbon layer through the photoconversion process on the branched-TiO_2 NWs. Furthermore, the output voltage of the branched-TiO_2/C structure reaches a saturation plateau around 60 s (Fig. 3d). In contrast, although with a relatively slower rate after 90 s of illumination, the output voltage of the branched-TiO_2/meso-C structure continues to increase for > 300 s, suggesting a more extended charge accumulation process for the branched-TiO_2/meso-C hybrid structure.

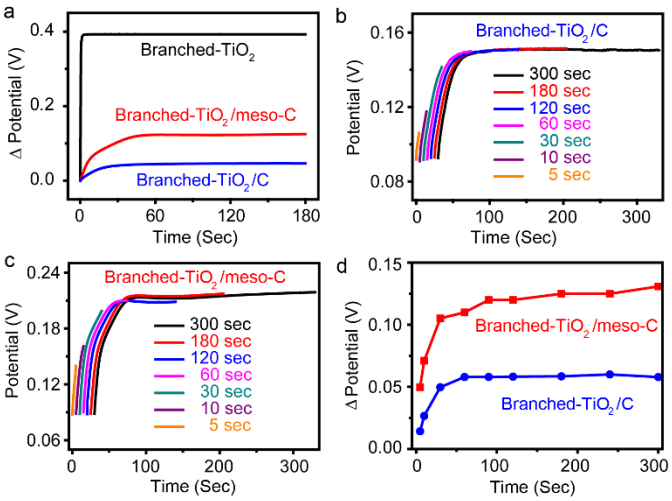

Fig. 3 Bias-free, photo-charging process. (a) Difference open circuit potential versus illumination (photo-charging) time of 3D branched-TiO_2 nanowires (black curve), branched-TiO_2/C (blue curve) and branched-TiO_2/meso-C (red curve) structures.

(b, c) Open circuit potential versus different illumination time of (b) 3D branched-TiO_2/C and (c) branched-TiO_2/meso-C hybrid structures. The x-axis (time) of each curve is offset successively by increasing 5 seconds for distinction. (d) Difference of open circuit potential versus illumination time of 3D branched-TiO_2/C (blue curve) and branched-TiO_2/meso-C (red curve) hybrid structures.

Galvanostatic discharge tests were further carried out to quantify the solar charged electric energy of these hybrid structures. For the bare branched-TiO_2 NWs, a quick discharging process is observed even under a small current of 10^{-5} A/g, indicating a very low capacitance, which only has a negligible variation with different light illumination (photo-charging) time from 5 to 240 s (Fig. 4a). For the branched-TiO_2/C structure, under a discharge current of 0.1 A/g, the discharging time increase to ~ 8 s, with the light illumination time (up to 60 s), suggesting the carbon layer is charged by the photo-generated holes (Fig. 4b). In contrast, for the branched-TiO_2/meso-C hybrid structure, under a discharge current of 0.1 A/g, the discharging time continues to increase to ~ 40 s, with the light illumination time of 300 s (Fig. 4c). The specific capacitances of these samples are further exhibited with respect to the light illumination (photo-charging) time (Fig. 4d). At a discharge current density of 0.1 A/g, the specific capacitance of the branched-TiO_2/meso-C hybrid structure is around 30 F/g, which is about 4 times of that of the branched-TiO_2/C structure (~8 F/g), under different light illumination up to 300 s. Comparatively, the branched-TiO_2/meso-C hybrid structure charged/discharged under an electrical field without solar irradiation shows a capacitance of ~ 54 F/g at a current density of 0.1 A/g (Fig. S5). Thus, the photo-charged capacitance of the branched-TiO_2/meso-C hybrid structure reaches ~ 60% of the electric-charged value. Although this capacitance value is lower than previous reports of electric field-charged mesoporous carbon materials (in the range of 40-200 F/g),[7,8] however, this branched-TiO_2/meso-C hybrid structure does not rely on the external electric power for charging the device, and can serve as an alternative means for unassisted, direct PEC conversion and energy storage.

Moreover, the rate performance of the branched-TiO_2/meso-C hybrid structure is further measured by varying the discharge current, while keeping the light illumination time as 180 s. The calculated capacitance is 27, 29.5, 30.8 and 23.4 F/g, for a discharging current density of 0.05, 0.1, 0.2 and 0.5 A/g, respectively (Fig. 4e), exhibiting the excellent rate performance of the photo-charged branched-TiO_2/meso-C EDLC device. Finally, the stability of the branched-TiO_2/meso-C EDLC is interrogated by repeated cycles of photo-charging at 100 mA/cm^2 and electrical discharging at 0.2 A/g. A stable specific capacitance of ~ 30 F/g is observed for over 50 cycles, without noticeable degradation (Fig. 4f), suggesting its excellent stability and superiority as photo-charging supercapacitors.

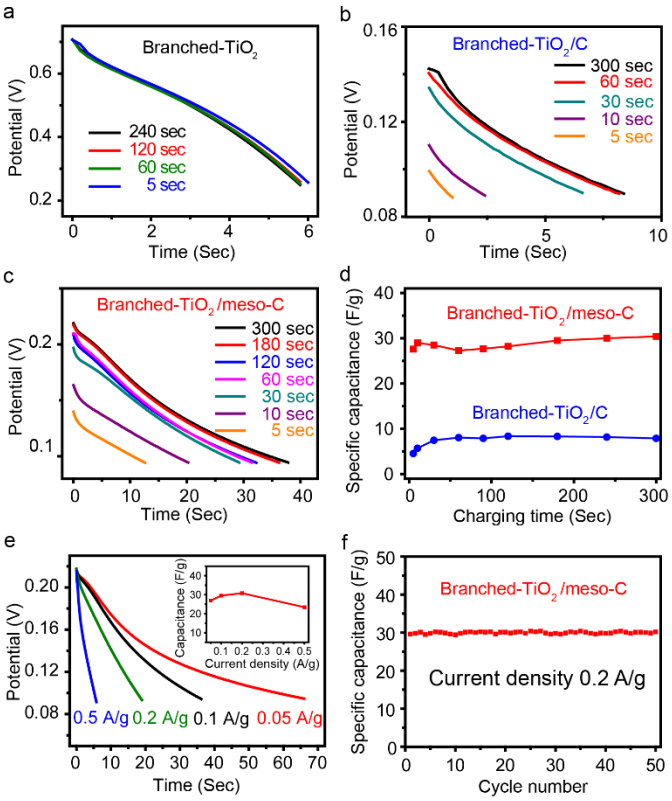

Fig. 4 Electrical discharging process. (a) Discharging curve of 3D branched-TiO_2 nanowires at a current density of 1×10^{-5} A. (b, c) Discharging curves at a current density of 0.1 A/g with different illumination (charging) time of (b) branched-TiO_2/C and (c) branched-TiO_2/meso-C hybrid structures. (d) Specific capacitance versus different illumination time of branched-TiO_2/C (blue curve) and branched-TiO_2/meso-C (red curve) hybrid structures. (e) Discharging curves at different current densities of branched-TiO_2/meso-C with an illumination time of 180 seconds. Inset: the summarized specific capacitance versus different current density. (f) Specific capacitance stability test of the branched-TiO_2/meso-C hybrid structures at a current density of 0.2 A/g.

CONCLUSIONS

In summary, we have demonstrated a 3D branched TiO_2/mesoporous carbon hybrid structure for unassisted, direct PEC conversion of solar energy with simultaneous electric energy storage. This hybrid structure takes full advantages of the unique traits of both 3D branched-TiO_2 in PEC activity and mesoporous carbon in electric storage, and can be robustly under 1-sun illumination and no external electric bias. A specific capacitance of over 30 F/g is obtained at a current density of 0.1 A/g, which is substantially higher than branched-TiO_2 NWs without carbon coating and also ~ 3 times higher than that of branched-TiO_2 NWs coated with nonporous carbon. The specific capacitance shows good stability under a series of discharging current densities varies from 0.05 to 0.2 A/g, and can be repeatedly photocharged-electrically discharged for > 50

cycles without noticeable degradation. Further design and optimization of the hybrid photoconversion/electric storage materials may open up a host of new opportunities in developing direct and efficient solar energy storage and utilization.

Acknowledgements

We thank the following funding agencies for supporting this work: the National Key Basic Research Program of China (2013CB934104), the Natural Science Foundation of China (21322311, 21473038, 21071033), the Science and Technology Commission of Shanghai Municipality (14JC1490500), the Doctoral Fund of Ministry of Education of China (20130071110031), the Program for Professor of Special Appointment (Eastern Scholar) at Shanghai Institutions of Higher Learning, and the Deanship of Scientific Research of King Saud University (IHCRG#14-102).

Notes and references

Laboratory of Advanced Materials, Department of Chemistry, Fudan University, Shanghai, 200433, China
E-mail: gfzheng@fudan.edu.cn
† These authors contributed equally.

Electronic Supplementary Information (ESI) available: Supporting figures, with additional SEM images, XRD spectra, N_2 sorption isotherms and pore diameter distribution curves, UV-Vis spectra, and charge/discharge data. See DOI: 10.1039/b000000x/

1 D, Pech, M.Brunet, H. Durou, P. Huang, V. Mochalin, Y. Gogotsi, P-L. Taberna, P. Simon, *Nat. Nanotech*. 2010, **5**, 651.
2 M. Kaempgen, C. K. Chan, J. Ma, Y. Cui, G. Gruner, *Nano Lett*. 2009, **9**, 1872.
3 D. N. Futaba, K. Hata, T. Yamada, T. Hiraoka, Y. Hayamizu, Y. Kakudate, O. Tanaike, H. Hatori, M. Yumura, S. Iijima, *Nat. Mater*. 2006, **5**, 987.
4 Z. Fan, J. Yan, L. Zhi, Q. Zhang, T. Wei, J. Feng, M. Zhang, W. Qian, F. Wei, *Adv. Mater*. 2010, **22**, 3723.
5 C. Liu, Z. Yu, D. Neff, A. Zhamu, B. Z. Jang, *Nano Lett*. 2010, **10**, 4863.
6 T. Wang, Z. Peng, Y. Wang, J. Tang, G. Zheng, *Sci. Rep.* 2013, **3**, 2693.
7 Y. Zhai, Y. Dou, D. Zhao, P. F. Fulvio, R. T. Mayes, S. Dai, *Adv. Mater*. 2011, **23**, 4828.
8 L. L. Zhang, X. S. Zhao, *Chem. Soc. Rev*. 2009, **38**, 2520.
9 M. Si, D. Feng, L. Qiu, D. Jia, A. A. Elzatahry, G. Zheng, D. Zhao, *J. Mater. Chem. A* 2013, **1**, 13490.
10 Y. G. Wang, H. Q. Li, Y. Y. Xia, *Adv. Mater*. 2006, **18**, 2619.
11 B. Kong, J. Tang, Z. Wu, J. Wei, H. Wu, Y. Wang, G. Zheng, D. Zhao, *Angew. Chem., Int. Ed*. 2014, **53**, 2888.
12 P. Yang, J. M. Tarascon, *Nat. Mater*. 2012, **11**, 560.
13 X. Feng, K. Zhu, A. J. Frank, C. A. Grimes, T. E. Mallouk, *Angew. Chem. Int. Ed*. 2012, **51**, 2727.
14 W. Guo, C. Xu, X. Wang, S. Wang, C. Pan, C. Lin, Z. L. Wang, *J. Am. Chem. Soc*. 2012, **134**, 4437.
15 W. Q. Wu, B. X. Lei, H. S. Rao, Y. F. Xu, Y. F. Wang, C. Y. Su, D. B. Kuang, *Sci. Rep*. 2013, **3**, 1352.
16 T. J. Kempa, R. W. Day, S-K. Kim, H-G. Park, C. M. Lieber, *Energy Environ. Sci.*, 2013, **6**, 719.
17 M. Xu, P. Da, H. Wu, D. Zhao, G. Zheng, *Nano Lett*. 2012, **12**, 1503.
18 Y. C. Pu, G. Wang, K. D. Chang, Y. Ling, Y. K. Lin, B. C. Fitzmorris, C. M. Liu, X. Lu, Y. Tong, J. Z. Zhang, Y. J. Hsu, Y. Li, *Nano Lett*. 2013, **13**, 3817.
19 R. H. Coridan, K. A. Arpin, B. S. Brunschwig, P. V. Braun, N. S. Lewis, *Nano Lett*. 2014, **14**, 2310.
20 L. Li, Y. Yu, F. Meng, Y. Tan, R. J. Hamers, S. Jin, *Nano Lett*. 2012, **12**, 724.
21 P. M. Rao, L. Cai, C. Liu, I. S. Cho, C. H. Lee, J. M. Weisse, P. Yang, X. Zheng, *Nano Lett*. 2014, **14**, 1099.
22 G. Wang, H. Wang, Y. Ling, Y. Tang, X. Yang, R. C. Fitzmorris, C. Wang, J. Z. Zhang, Y. Li, *Nano Lett*. 2011, **11**, 3026.
23 J. Shi, Y. Hara, C. Sun, M. A. Anderson, X. Wang, *Nano Lett*. 2011, **11**, 3413.
24 I. S. Cho, Z. Chen, A. J. Forman, D. R. Kim, P. M. Rao, T. F. Jaramillo, X. Zheng, *Nano Lett*. 2011, **11**, 4978.
25 X. Sheng, D. He, J. Yang, K. Zhu, X. Feng, *Nano Lett*. 2014, **14**, 1848.
26 Z. Yin, Z. Wang, Y. Du, X. Qi, Y. Huang, C. Xue, H. Zhang, *Adv. Mater*. 2012, **24**, 5374.
27 M. T. Mayer, C. Du, D. Wang, *J. Am. Chem. Soc*. 2012, **134**, 12406.
28 L. Zhao, X. Chen, X. Wang, Y. Zhang, W. Wei, Y. Sun, M. Antonietti, M-M. Titirici, *Adv. Mater*. 2010, **22**, 3317.
29 Z. Jiang, Y. Tang, Q. T ay, Y. Zhang, O. I. Malyi, D. Wang, J. Deng, Y. Lai, H. Zhou, X. Chen, Z. Dong, Z. Chen, *Adv. Energy Mater*. 2013, **3**, 1368.
30 M. J. Kenney, M. Gong, Y. Li, J. Z. Wu, J. Feng, M. Lanza, H. Dai, *Science* 2013, **342**, 836.
31 X. Xia, J. Luo, Z. Zeng, C. Guan, Y. Zhang, J. Tu, H. Zhang, H. J. Fan, *Sci. Rep*. 2012, **2**, 981.
32 Y. Wang, J. Tang, Z. Peng, D. Jia, B. Kong, A. A. Elzatahry, D. Zhao, G. Zheng, *Nano Lett*. 2014, **14**, 3668.
33 Z. Li, C. Yao, Y. Yu, Z. Cai, X. Wang, *Adv. Mater*. 2014, **26**, 2262.
34 H. Chen, C. Chen, R. Liu, L. Zhang, J. Zhang, D. P. Wilkinson, *Chem. Soc. Rev*. 2012, **41**, 5654.
35 D. Feng, Y. Lv, Z. Wu, Y. Dou, L. Han, Z. Sun, Y. Xia, G. Zheng, D. Zhao, *J. Am. Chem. Soc*. 2011, **133**, 15148.